IDENTIFICATION OF THREE DOMINANT RAINFALL REGIONS WITHIN INDONESIA AND THEIR RELATIONSHIP TO SEA SURFACE TEMPERATURE

EDVIN ALDRIAN[a,*,†] and R. DWI SUSANTO[b]

[a] *Max Planck Institut für Meteorologie, Bundesstrasse 55, Hamburg 20146, Germany*
[b] *Lamont Doherty Earth Observatory of Columbia University, Palisades, NY 10964-8000, USA*

ABSTRACT

The characteristics of climatic rainfall variability in Indonesia are investigated using a double correlation method. The results are compared with empirical orthogonal function (EOF) and rotated EOF methods. In addition, local and remote responses to sea-surface temperature (SST) are discussed. The results suggest three climatic regions in Indonesia with their distinct characteristics. Region A is located in southern Indonesia from south Sumatera to Timor island, southern Kalimantan, Sulawesi and part of Irian Jaya. Region B is located in northwest Indonesia from northern Sumatra to northwestern Kalimantan. Region C encompasses Maluku and northern Sulawesi. All three regions show both strong annual and, except Region A, semi-annual variability. Region C shows the strongest El Niño–southern oscillation (ENSO) influence, followed by Region A. In Region B, the ENSO-related signal is suppressed. Except for Region B, there are significant correlations between SST and the rainfall variabilities, indicating a strong possibility for seasonal climate predictions. March to May is the most difficult season to predict the rainfall variability. From June to November, there are significant responses of the rainfall pattern to ENSO in Regions A and C. A strong ENSO influence during this normally dry season (June to September) is hazardous in El Niño years, because the negative response means that higher SST in the NIÑO3 of the Pacific region will lower the rainfall amount over the Indonesian region. Analyses of Indonesian rainfall variability reveal some sensitivities to SST variabilities in adjacent parts of the Indian and Pacific Oceans. Copyright © 2003 Royal Meteorological Society.

KEY WORDS: Indonesian rainfall; monsoon; ENSO influence; regionalization; SST

1. INTRODUCTION

There have been several studies on rainfall variability over the Indonesian archipelago and its relation to large-scale climatic phenomena such as El Niño–southern oscillation (ENSO; Philander, 1983; Kirono *et al.*, 1999) and monsoon (Braak, 1921; Wyrkti, 1956; Sukanto, 1969; Hackert and Hastenrath, 1986; McBride, 1999; Haylock and McBride, 2001). Because Indonesia is as large as the USA, consists of more than 17000 islands, is located between the Pacific and Indian Oceans and between the Asian and Australian continents, the influence of these large-scale climate phenomena varies across the region due to island topography and/or ocean–atmosphere fluxes, which are imposed by sea-surface temperature (SST) variability. To investigate the relationship of rainfall to the monsoon and ENSO, we need not only long-term rainfall time series but also more stations to improve the resolution of the spatial variability over the entire Indonesian region. Better spatial and temporal resolutions of the rainfall will allow a more quantitative understanding of the causal links of Indonesian rainfall to larger scale climate features. Hence, it is important to study the climatic rainfall

---

* Correspondence to: Edvin Aldrian, Max Planck Institut für Meteorologie, Bundesstrasse 55, Hamburg 20146, Germany; e-mail: aldrian@dkrz.de
† On leaving the Agency for the Assessment and Application of Technology, BPP Teknologi, Jakarta, Indonesia.

variability over Indonesia using more complete data sets and appropriate statistical tools. Analyses using a new double correlation method and two already established methods, i.e. the covariance empirical orthogonal function (EOF) and the rotated EOF, will be discussed here.

Using monthly rainfall data from only 33 stations over 49 years from 1950 to 1998, Kirono *et al.* (1999) noted that during the 1997–98 El Niño, virtually the entire country had rainfall below the 10th percentile, with many stations recording the lowest rainfall on record. Haylock and McBride (2001) extended the studies using rainfall data from 63 stations from 1950 to 1998 to determine the spatial coherence of wet season anomalies. Using an average of 43 rainfall stations from a subset of Haylock and McBride (2001) data into a single value/index rainfall time series, Hendon (2003) found that Indonesian rainfall is coherent and strongly correlated to ENSO variations in the Pacific basin. Given the large size of the Indonesian archipelago, we definitely need more stations to represent the rainfall variability adequately over the region. In Section 3 we will show that, based on annual variability, Indonesia has three distinct rainfall regions. A simple average over the whole Indonesian region disregards the wide range of rainfall variability. A single regional index may be valid only if intra-regional contrasts in rainfall regime do no exist (McGregor, 1992).

Previous investigators have demonstrated that the SST anomalies over Indonesia and northern Australia are closely related to the ENSO phenomenon (Newell *et al.*, 1982; Rasmusson and Carperter, 1982; Nicholls, 1983, 1984, 1995; Gutman *et al.*, 2000). The relationship between Indonesian SST and ENSO and the tendency for the former to lead east Pacific SST suggests that Indonesian SST might provide forecasts of Indian monsoon with longer lead times than is possible using either Darwin pressure tendencies (Shukla and Paolino, 1983) or the east Pacific SST (Rasmusson and Carperter, 1982). Using global rainfall and SST data for 1979–98, Lau and Wu (1999, 2001) demonstrated the importance of regional processes in affecting the Australian–Asian summer monsoon rainfall variability. On average, ENSO-related basin-scale SSTs account for 47% of the rainfall variability, and regional processes account for an additional 16%. The rest accounts for decadal, biennial and small-scale variabilities. On the other hand, Hendon (2003) suggested that NIÑO3-4 SST variability accounts for 50% of the variance of the all-Indonesian rainfall and that SST variability over the Indian Ocean accounts for 10–15%. The results suggest that, in order to improve seasonal-to-interannual predictability of the Australian–Asian monsoon, we need to investigate and exploit not only the relationship between monsoon and El Niño, but also internal regional processes coupled with the local monsoon. Our study investigates the relation between SST in both the Pacific and Indian Oceans (including local SST within the Indonesian seas) and its influence on the rainfall variability in Indonesia.

Given the complexity of the land–sea distribution in the region and the many factors affecting the rainfall variability, such as orography and local SST (Wyrki, 1956), more complete data sets and a suitable statistical method to delineate smaller more homogeneous regions are needed. In this paper, we introduce a regionalization method, the 'double correlation method' (DCM), based on the annual rainfall cycle or the annual mean variability. The first regionalization attempt for this region was done by Wyrtki (1956), when he divided the Indonesian waters into nine subregions. The main objective of this study is to present an objective method for a division of Indonesian rainfall variability using the DCM. In addition, the roles of local and remote seas are investigated. In the Section 2 we shall describe the data and the DCM. Section 3 discusses the results based on the DCM, compares them with the covariance and rotated EOF methods and then evaluates the responses of each region to SST in local and surrounding seas. Finally, Section 4 contains the overall discussion and conclusions.

2. DATA AND METHODS

The study area covers the Indonesian archipelago, an area between 15°S to 8°N and 90 to 140°E (inset of Figure 1). There are thousands of secondary meteorological stations in the region; however, only 884 rain gauges from the primary stations within the region are available in the World Meteorological Organization–National Oceanic and Atmospheric Administration (WMO–NOAA) project on the Global Historical Climatology Network database (GHCN; Vose *et al.*, 1992). Among those are 526 stations from the Indonesian Meteorological & Geophysical Agency (BMG). We use the GHCN precipitation data version
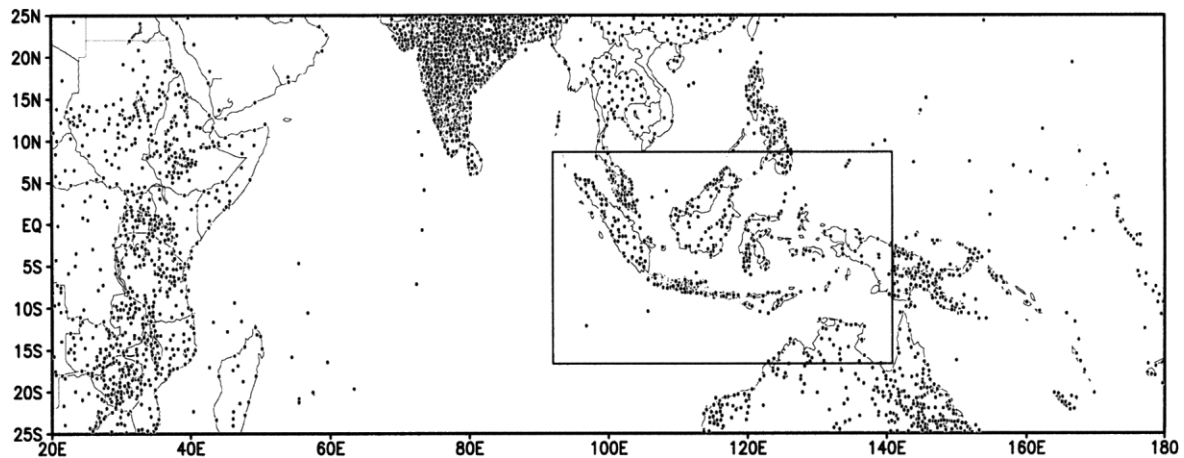
Figure 1. The distribution of rain gauge stations over 20–180 °E, 30 °S–30 °N with 5419 stations and over the Indonesian archipelago over 15 °S–8 °N, 90–140 °E (inset) with 884 stations. All analyses except the EOF and VARIMAX methods use the inset domain

2, which provides monthly rainfall data until 1993. After 1993, only 60 stations are available within the Indonesian region via the Global Telecommunication System, and no data are available after 1996 (Vose, 2002, personal communication). The data have passed some quality control tests, including the homogeneity test, before they are incorporated into GHCN (Peterson *et al.*, 1998). Since some stations have data only since 1960, in this study, we use monthly rainfall data from 1961 to 1993. Using the Cressman (1959) objective analysis, these data (all regional rainfall data shown in Figure 1) are then gridded into the T106 resolution of the global climate models, which corresponds to a spatial resolution of 1.125° latitude by 1.125° longitude.

The gridded SST data from the Global Ice and Sea Surface Temperature data set (GISST2; Rayner *et al.*, 1996) version 2.3b are used in this study. This data set is compiled from SST observations from 1871 to the present, with a spatial resolution of 1°. To investigate the roles of SST from local and remote seas on rainfall variability, we select SST data to have the same period as the rainfall data from 1961 to 1993 only.

Owing to the high spatial variability of the Indonesian rainfall, we need a statistical method that can reduce the bias error. It will be shown that the DCM provides better results in classifying the climate division than the EOF method. A region that consists of grid cells with similar annual cycles is likely to respond specifically and homogeneously to a climate phenomenon. The regions applied must be distinct (no overlap) from their neighbours and each should represent the dominant climate phenomenon acting on it. One could use a simple box with a definite longitudinal and latitudinal boundary to set a region. This approach is biased to some extent because many climatic factors, as previously mentioned, interplay over the region. The DCM could reduce this bias.

With the DCM, we look for a region in which the annual cycles of its grid cells are correlated among themselves by more than a certain threshold value. To make it more efficient, rather than correlating all grid cells to each other, we first select some reference cells. Second, we correlate all other cells to these reference cells based on their annual cycles. Cells that are correlated above a certain threshold value are selected to belong to a region. Third, we correlate all grid cells again with the mean annual cycle of the resulting region using the same threshold value. The aim of the second correlation is to produce a region independent of the choice of the reference grid. The threshold value should be the highest correlation value that produces no overlapping boundaries. In this paper, the threshold value chosen is $r^2 \geq 0.67$ with a 99% confidence level, assuming 33 degrees of freedom (i.e. assuming each year is independent). Thus, with double correlations, the level of significance is much higher than a single correlation. With such a high degree of significance, the choice of reference cells is not difficult and not very relevant for the result.

To fulfil the above criteria, a simplified procedure has been carried out as follows. First, we selected 100 rain gauge stations with a high quality record (with the least missing data). These were gridded at the T42 resolution (2.8125°). The 100 stations are widely distributed over Indonesia and cover 48 land grid areas.

Then, using their mean annual cycle, we set up a 48×48 cross-correlation matrix, from which we classified five clusters of strong correlations that are attributed to five climatic regions. We then selected our reference cells from these regions to start the DCM at the T106 resolution using the whole data set. All regions are bounded by the same coordinates ($15\,°S–8\,°N$, $90–141\,°E$).

3. RESULTS

The results from the DCM are three climate regions, as shown in Figure 2. Region A (solid line) covers south and central Indonesia from south Sumatera to Timor Island, parts of Kalimantan, parts of Sulawesi, and parts of Irian Jaya. Region B (short dashed line) is located in northwest Indonesia and covers the northern part of Sumatera and the northwestern part of Kalimantan. Region C covers Maluku and parts of Sulawesi (close to the western Pacific region). With a threshold value $r^2 \geq 0.67$ we obtain a clear boundary among regions without overlapping, although there are some discontinuities (intermediate region). Region A, which covers the largest area, is the dominant pattern over Indonesia. Based on analysis of the amplitude and phase of annual oscillation from the pentad-mean rainfall amounts average, Hamada *et al.* (2002) classified Indonesia into four climatological regions. They found similar characters of our three regions and the intermediate region with no clear rainy and dry seasons.

The mean annual rainfall cycles of each region and their interannual standard deviations are described in Figure 3. From this figure, each region has its own distinct feature. Region A has one peak and one trough and experiences strong influences of two monsoons, namely the wet northwest (NW) monsoon from November to March (NDJFM) and the dry southeast (SE) monsoon from May to September (MJJAS). Region B has two peaks, in October–November (ON) and in March to May (MAM). Those two peaks are associated with the southward and northward movement of the inter-tropical convergence zone (ITCZ). Davidson and co-workers (Davidson *et al.*, 1984; Davidson, 1984) described in detail the ITCZ movement in this region in boreal winter. There is no clear reason why the peak in ON is much higher than that of MAM. There is a possible influence of a cool surface current coming from the north out of the South China Sea during January–March (Wyrtki, 1961) that suppresses the rainfall amount. Otherwise, the annual cycle of Region B would be similar to that of Region A. Region C has one peak in June to July (JJ) and one trough
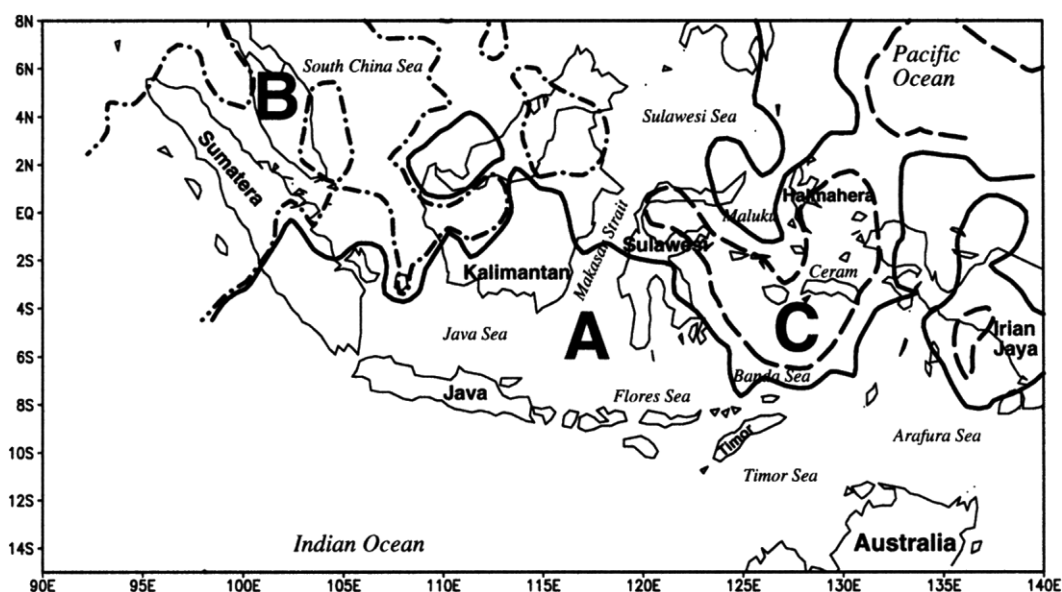

Figure 2. The three climate regions according to the mean annual patters using the DCM. Indonesia is divided into Region A in solid line, Region B in short dashed line and Region C in long dashed line
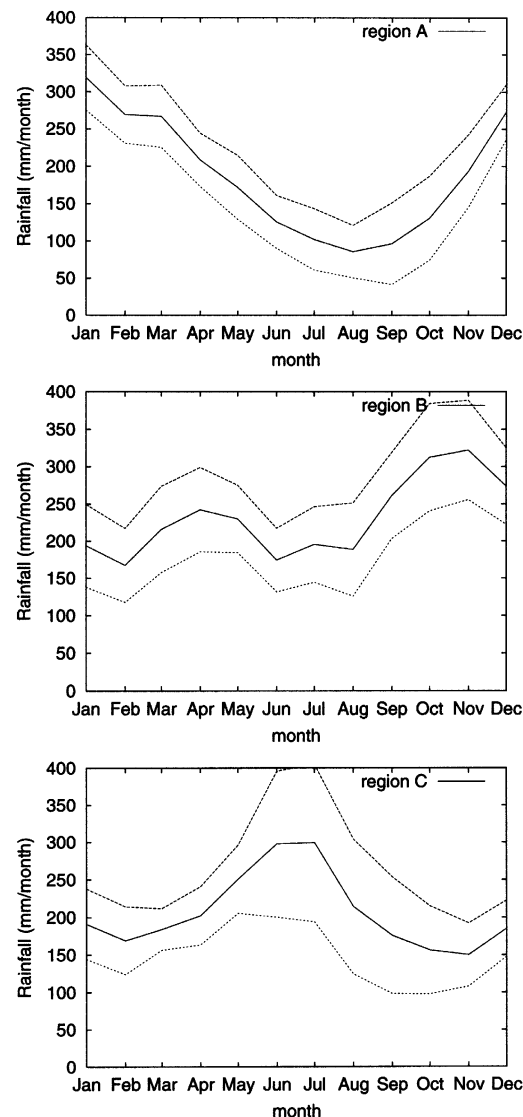
Figure 3. The annual cycles of the three climate regions (solid lines) using the DCM. Dashed lines indicates one standard deviation (σ) above and below average

(November–February). The JJ peak in Region C is about 300 mm/month, whereas the peaks in Regions A and B are 320 mm/month and 310 mm/month respectively. The minimum in Region A is the lowest and reaches a mean below 100 mm/month. Thus, Region A is the driest region during the dry season in July–September and the wettest region in December.

Region C has one peak in the middle of year (JJ), whereas the other two regions have their peaks near the end/beginning of the year. There is a strong evidence of the possibility of ocean influence in Region C. Region C, or Maluku, is along the eastern route of the Indonesian Throughflow (ITF; a water passage from the Pacific Ocean to the Indian Ocean via Indonesian seas; Gordon and Fine, 1996). The ITF flows mainly through the Makassar Strait with a small part flowing through the Maluku Sea (Gordon *et al.*, 1999). The ITF in Maluku brings sea surface currents from the warm pool area, which is located northeast of Irian Jaya Island (New Guinea). As suggested from the distribution of the region itself, there is some part of this region that lies north of Irian Jaya. Hence, the SST over Maluku is determined mainly by the condition over the

warm pool. During the wet season (NDJFM) the sun position is in the Southern Hemisphere. The ITF brings cooler water from the warm pool to the Maluku Sea (Godfrey, 1996; Morey *et al.*, 1999). This cooler SST inhibits the formation of a convective zone. On the other hand, during the dry season (MJJAS) the warm SST enhances the convective zone. Hence, we obtain the peak in May–July and the trough in October–January.

The standard deviation in Region A is smaller throughout the whole year, which indicates a strong coherent pattern. On the other hand, the other two regions have stronger interannual cycles than Region A. The homogeneous pattern in Region A indicates the wide extent of the dry season, which reaches all Java and the Lesser Sunda Islands, Sumatera and part of Kalimantan.

3.1. The covariance EOF and the VARIMAX method

Because the covariance EOF and rotated EOF methods (von Storch and Zwiers, 1999) are widely used to delineate subregions according to a common eigen property, we compare the DCM with these methods. In this paper, the VARIMAX rotation (Kaiser, 1958) was used as a method for rotating the EOF. The EOF method is capable of extracting the principal components (PCs) of patterns in a time series. Each of the PCs will be orthogonal to the others. The first PC (PC1) will be the most dominant pattern and it explains most of the variance. Then PC2 will be the second most dominant PC, followed by PC3, etc. In total, there will be the same number of PCs as the number of data in the time series. The original data set will be the combination of all PCs multiplied by the time series of their respective coefficients' time series.

Since the EOF calculation is sensitive to the domain size, especially in a small area, we use a much larger domain (25 °S–25 °N, 20–180 °E) from the GHCN data set (Figure 1) for the EOF and VARIMAX method to minimize the sensitivity of our Indonesian domain (the inset box in Figure 1). The spatial pattern of PC1 and PC2 of the EOF method is given in Figure 4. PC1 and PC2 respectively explain 30.08% and 8.09% of all variances and represent the annual and semi-annual patterns. Those two PCs only explain less than half of the total variance because we took the whole data set of 33 years. The rest explain non-annual patterns, whereas we are aiming at only the annual patterns for our regionalization. The distribution of apparent regions in PC1 resembles that of the DCM. Regions A, B and C from the DCM are approximately represented in PC1 by
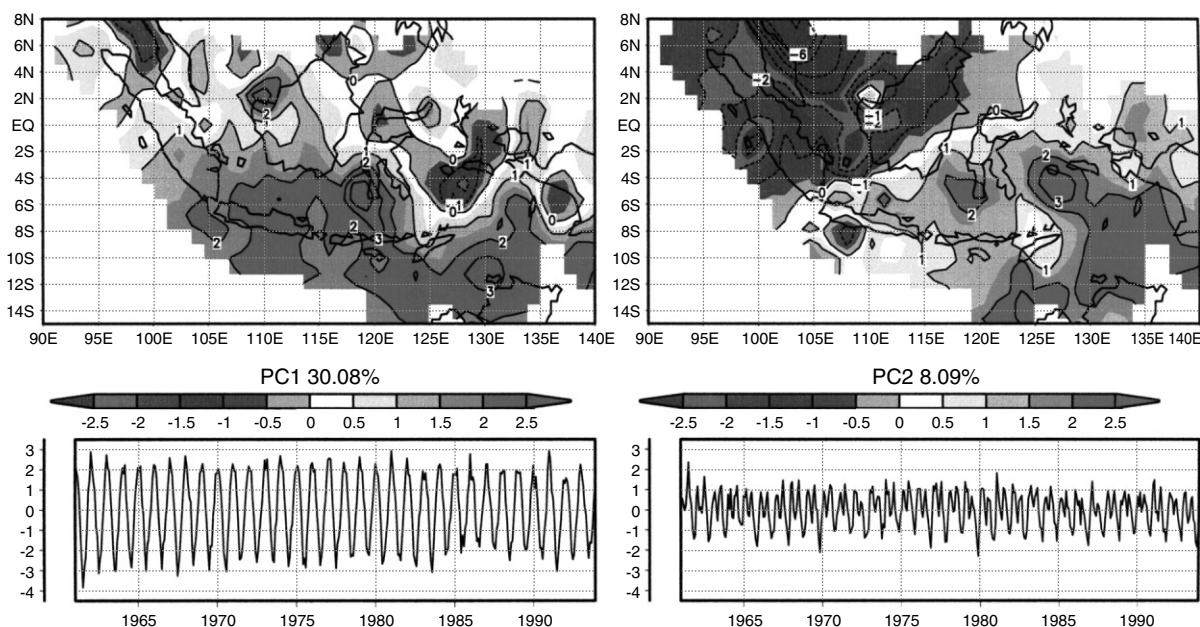

Figure 4. The first two PCs of the EOF method using the same data set as the DCM. Regions A and C in Figure 2 are present in PC1 and Region B (not obvious) in PC2 with a broader intermediate region in east Indonesia between Regions A and C. Below are the coefficient time series of each PC, which explain that PC1 and PC2 are the annual and the semi-annual patterns

the areas with values above 1.0, between 0 and 1.0 and negative values respectively. The opposite sign of Regions A and B with respect to Region C for the EOF method implies the opposite annual cycle (as already seen in Figure 3). The main differences between the results of both methods are the border of Region B and the intermediate region in the east. The annual cycle of the intermediate region would be a mixture between pattern A and C with two peaks and minimums and a flat annual cycle.

Figure 5 shows the first two PCs from the rotated EOF using the VARIMAX method. PC1 and PC2 explain 23.47% and 12.65% of all variances respectively. Those PCs are calculated using the first 100 PCs (which explain 90.7% of all variances) of the EOF method. Again, Region C corresponds to the region of PC1 with negative loadings, whereas the border of Region A is obvious only in the eastern part. Region B has values above 0.5 of PC2. The presence of Region B in PC2 is understandable, because Region B has similar semi-annual characteristics to PC2.

In summary, it is difficult to judge whether the EOF or the VARIMAX method gives a better regionalization. With the EOF method, the boundaries of Regions A and C exist in PC1, but the boundary of Region B does not, and the boundaries of Regions B and C exist respectively in PC1 and PC2 of the VARIMAX method, but the western boundary of Region A does not. Because EOF analysis is purely a statistical tool, prior knowledge of the physical processes is important in the interpretation of the results. Sometimes, patterns derived from EOF analyses can be misleading and associated with very little physics (Dommenget and Latif, 2002).

3.2. Spectral analysis of the EOF and the DCM

To clarify which frequency dominates the rainfall pattern, we investigated the power spectra of each region from the DCM and each coefficient of the EOF and the VARIMAX methods. Figure 6 illustrates the power spectra of rainfall area average from the three regions and all Indonesia (a box bounded by 15 °S, 8 °N, 90 °E and 140 °E). The spectra are shown with a logarithmic time scale for periods from 2 months to 30 years. Important time scales are indicated along the *x*-axis. Those important periods are 0.25, 0.5, 1, 2, 4–7 and 10 years, which represent 3-monthly, semi-annual, annual, biennial, ENSO-related and decadal
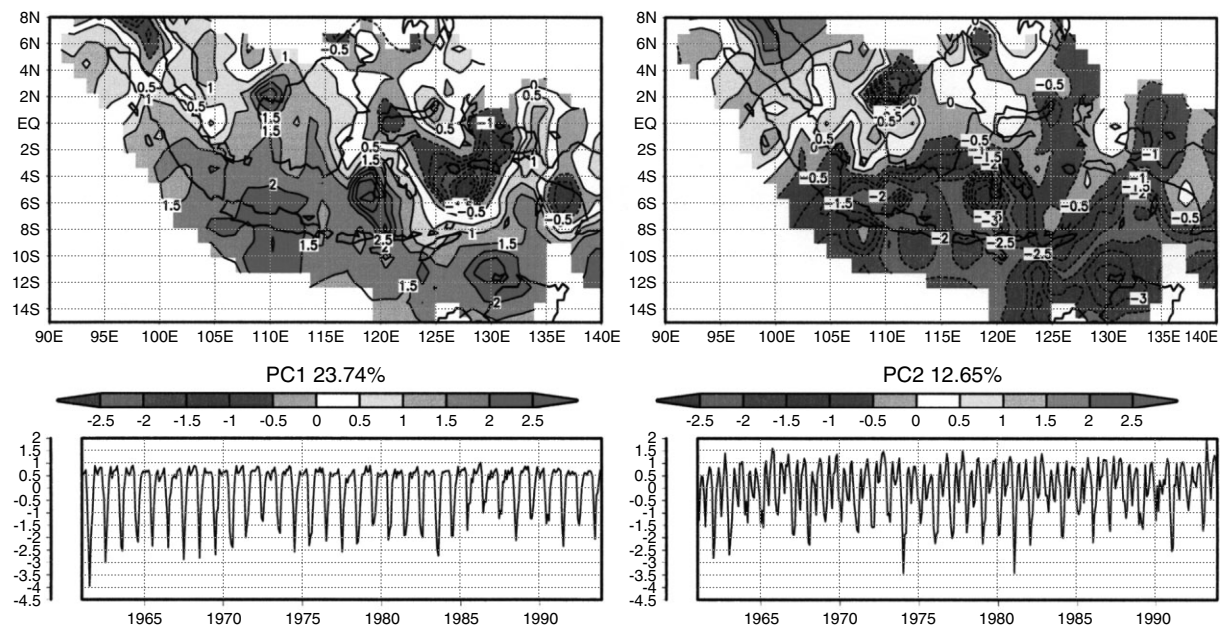

Figure 5. The first two PCs of the rotated EOF method using the first 100 PCs (explain 90.7% of all variances) from the unrotated EOF. Regions A and C are indicated with boundaries >0.5 and <0.0 respectively in PC1. Region B is present in PC2 with boundary >0.5. Below are the coefficient time series of each PC, which explain that PC1 and PC2 are the annual and the semi-annual patterns
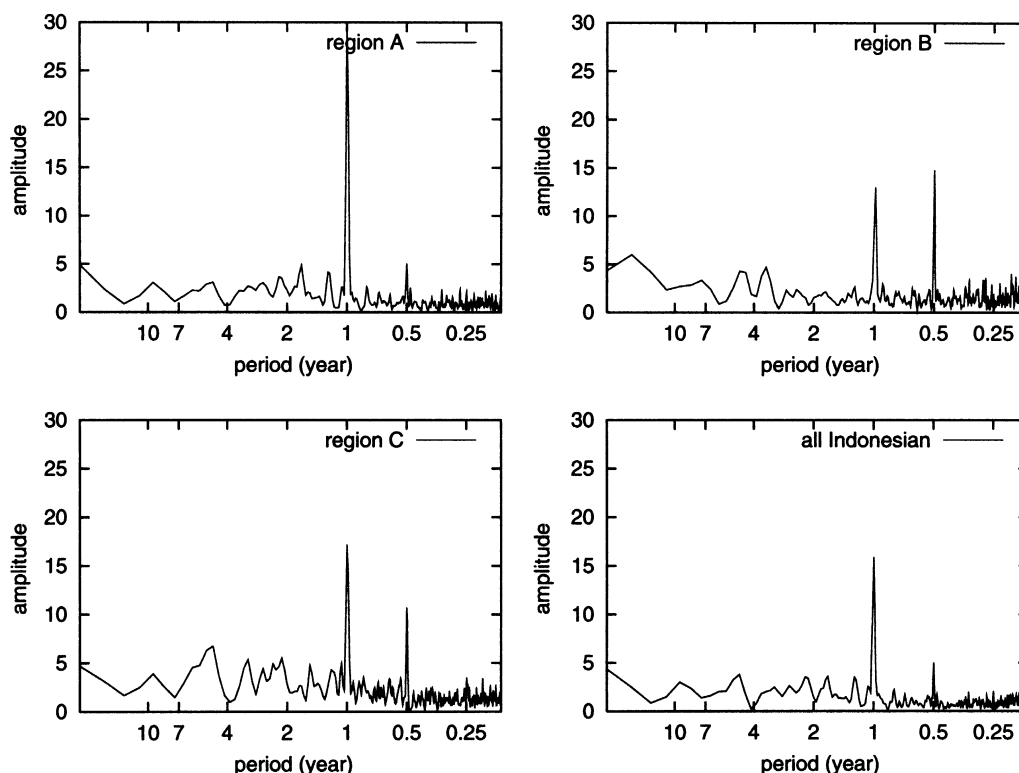
Figure 6. The frequency spectra of the three regions and the all-Indonesia region after smoothing with 1−2−1 convolution

signals respectively. Since the spectra are white noises or AR(0) processes (a time series whose statistics (e.g. mean, variance, etc.) do not depend upon a fixed starting point, but only on time separation), all peaks are significant.

The spectrum of Region A has a strong annual signal. It dominates the overall variability with a value more than six times that of any other maximum. The strongly prevailing annual signal of Region A suggests a strong homogeneous pattern, as also shown by a small standard deviation of its annual cycle in Figure 3.

The spectrum of Region B has strong annual and semi-annual signals, with the semi-annual one being slightly stronger than the annual. The strong semi-annual signal is evident from the annual cycle, because of the presence of two peaks and two minimums (Figure 3). Interestingly, there is a remarkable signal in a period of more than a decade. This may be associated with the decadal-scale fluctuation of the west Pacific anticyclone (Lau and Wu, 2001).

The spectrum of Region C has two strong peaks and several weaker ones. Similar to Region A, the annual cycle dominates the rainfall variability of this region. The semi-annual signal designates the presence of two peaks in the annual cycle. From the annual cycle, there is a peak in May−July, and a smaller peak in November−January. Other notable signals that contribute to the high standard deviations to the annual cycle of Region C are the biennial and ENSO-related signals (4−7 years). As shown in Figure 3, Region C has large standard deviations from June to November.

Overall, the three regions show both strong annual signals and, except for Region A, semi-annual signals. This is an indication that the DCM works well in isolating signals in a region based on its annual cycle. Region C shows the strongest ENSO signal, followed by Region A. In Region B, the ENSO-related signal is suppressed, which is indicated by a minimum instead of a peak in the period range 4−7 years. The spectrum of all-Indonesian rainfall shows the dominance of the annual and semi-annual signals (monsoonal) type of climate. The annual signal is three times stronger than the semi-annual one. Low-frequency signals (period more than 1 year) are stronger than high-frequency signals (period less than 1 year). The strong decadal

signals in all four spectra are in agreement with weak low-frequency variabilities in EOF coefficients of PC1 (Figures 4 and 5).

The spectra of the first two PC coefficients from both the EOF and VARIMAX methods are shown in Figure 7. The units of the *y*-axes are arbitrary. It is impossible to compare the amplitude values from the two methods directly. However, our interest is only in the locations of significant peaks. The two spectra of EOF show strong annual and semi-annual signals. The low-frequency signals (period more than 1 year), the semi-annual signal and the intraseasonal signal with a period of 4 months in PC1 are overshadowed by the strong peak of the annual signal. Thus, compared with the result of the DCM, the EOF method gives a stronger annual signal. Although the three regions from the DCM are also obvious in PC1, the resulting spectra are different. The VARIMAX method shows both the annual and semi-annual signals in the first two spectra. The signal strength is reduced from the annual, semi-annual, and intra-monthly signals. The spectra of PC2 derived from both the EOF and the rotated EOF methods are comparable to that of Region B, which shows annual and semi-annual signals.

Based on our results, the DCM can be used to regionalize climate variability based on the annual rainfall cycle. The DCM produces clear boundaries and indicates the dominance of the annual signal (and some extent the semi-annual signal) in their spectra. If we compare the all-Indonesia spectrum with those of each PC, only PC1 from the VARIMAX method gives a comparable result. The spectrum of the all-Indonesia region exhibits particularly strong annual and semi-annual signals. One may argue that the EOF analysis was done on the basis of monthly data, whereas our DCM was done on the basis of annual cycles. However, we utilized only the annual and semi-annual components of the EOF and the VARIMAX methods. It is possible to do the DCM with the whole monthly data set, with the consequence of a lower threshold value for the same significance level. The results will differ according to the variability in each region. Regions with high
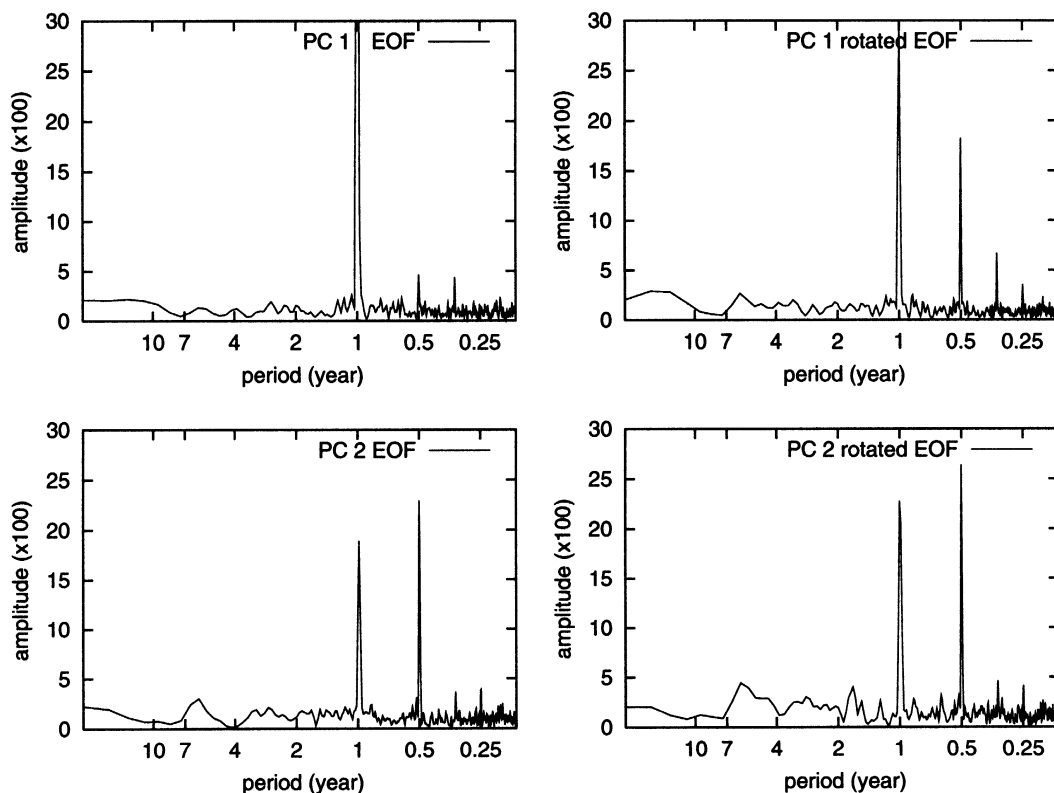

Figure 7. The frequency spectra of the first two PCs of the EOF method (left) and rotated EOF method (right) after smoothing with 1–2–1 convolution. PC1 EOF has an overflow value of 64.9 in the period of 1 year

variabilities, such as Region C, would not receive a comparable boundary as by the method applied here. The DCM is optimized in classifying regions according to their mean annual cycles. The high significance level of the threshold value contributes to regions with highly correlated grid cells. One major drawback of the method is the intermediate region. As stated before, the annual cycle of this region will be a flat annual one with two small peaks and two small minimums.

3.3. Local SST responses

We are interested in semi-annual and annual cycles of rainfall, the prominent time scales in this region. Therefore, we also investigated the rainfall response to SST in order to understand sea–air interactions locally and regionally. With regard to local SST responses, we selected three ocean regions, or boxes, bounded by a certain longitude and latitude from the three climate regions. The boxes chosen lie inside Regions A, B and C: South Maluku or Timor Sea (15–5 °S, 120–135 °E) for Region A, the South China Sea (1.5 °S–8 °N, 102–110 °E) for Region B and the Maluku Sea (6 °S–2 °N, 122–135 °E) for Region C. Figure 8 shows the scatter plots of rainfall versus local SST grouped by month for 33 years of monthly data (1961–93).

In Region A, the rainfall is clustered by month in the temperature range from 25.6 to 30.3 °C and shows an SST-related function, as previously suggested by Bony *et al.* (1997a,b) and Lau *et al.* (1997). They showed that, below 29.6 °C, the rainfall amount increases with SST; however, the increase is not linear. In contrast, above 29.6 °C the increase of local SST causes a decrease in the maximum rainfall amount. There is a clear distinction between the dry and the wet seasons. The dry season (MJJAS) SST is less than the wet season (NDJFM) SST. Both the SST and the rainfall amount decrease from January to August and increase from August to December, as indicated by the mean annual cycle in Figure 3. The rainfall in each month varies less in the dry season, especially in comparison to the wet season months in January and February. However, the majority of rainfall is distributed in narrow bands on both axes. This is in agreement with our previous result, which shows small standard deviations in the annual cycle of Region A all year long.

In Region B there is no clear rainfall–SST relationship, especially from October to March. In December–February (DJF), high precipitation amounts exist at low local SSTs, whereas in other regions the SSTs are high in DJF. The rainfall is scattered from 25.5 to 30.5 °C and from as low as 38 to 741 mm/month. The range of SST in each month in this region is also high, reaching almost 3 °C (January–March) compared with 1.5 °C in Region A. From April to September the data scatter less. The absence of a clear relationship between rainfall and SST in Region B suggests that the rainfall is independent of local ocean temperature and its variability. Possibly, strong atmospheric forcing may play some role here.

Compared with the two Regions A and B, Region C has the narrowest range in both axes, especially in December–February. The rainfall is distributed from 27 to 30 °C and from 14 to 375 mm/month. There seems to be some weak relationship between SST and rainfall in Region C, but this is less obvious than in Region A. The scatter of rainfall amount is high from June to September, as these months also show high standard deviations (Figure 3).

In general, relationships between local SST and rainfall appear in Region A and are less obvious in C. It is important to investigate further other atmospheric factors that govern the rainfall pattern in Region B. This result is quite surprising, because the area of our investigation is the maritime continent, which is surrounded by oceans.

3.4. Seasonal and remote SST responses

In this subsection we analyse rainfall responses from the three regions to remote SST on a seasonal basis, i.e. for DJF, MAM, June–August (JJA) and September–November (SON). DJF represents the peak of the northwest Australia–Asia monsoon, and JJA represents the peak of the southeast Australia–Asia monsoon. Both MAM and SON represent monsoon transitions. Our analysis covers major oceans surrounding Indonesia up to the NIÑO3 region (5 °S–5 °N, 150–90 °W) in order to see the ENSO response. The responses will be based on the correlation values between seasonal rainfall in each region and SST. Only correlation values above a certain significance level are presented.
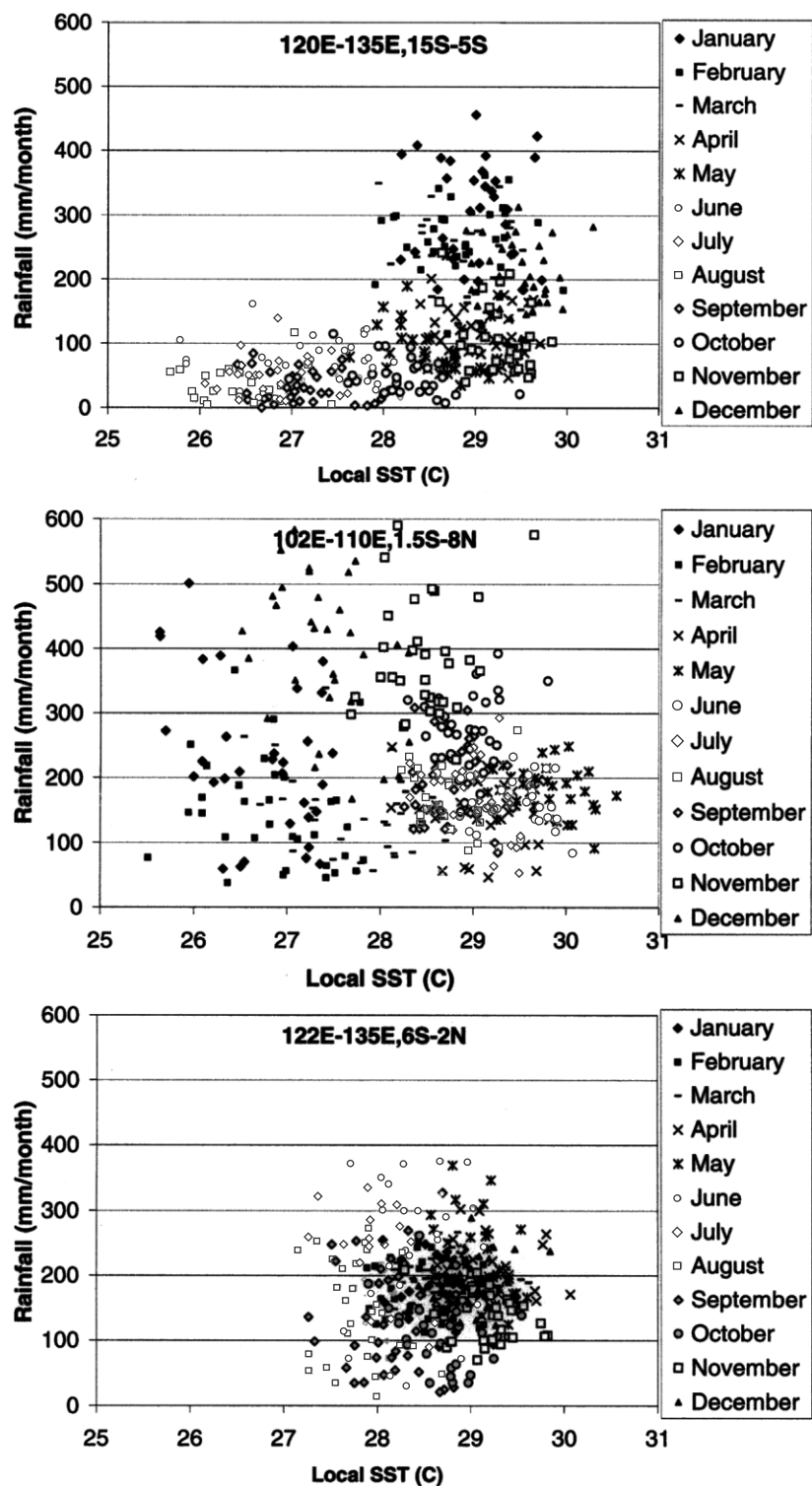
Figure 8. The monthly precipitation versus local SST patterns of the seas represent the three regions. Region A (top) is represented by the Timor Sea, Region B (middle) by the South China Sea and Region C (bottom) by the Maluku, Ceram and Halmahera Seas
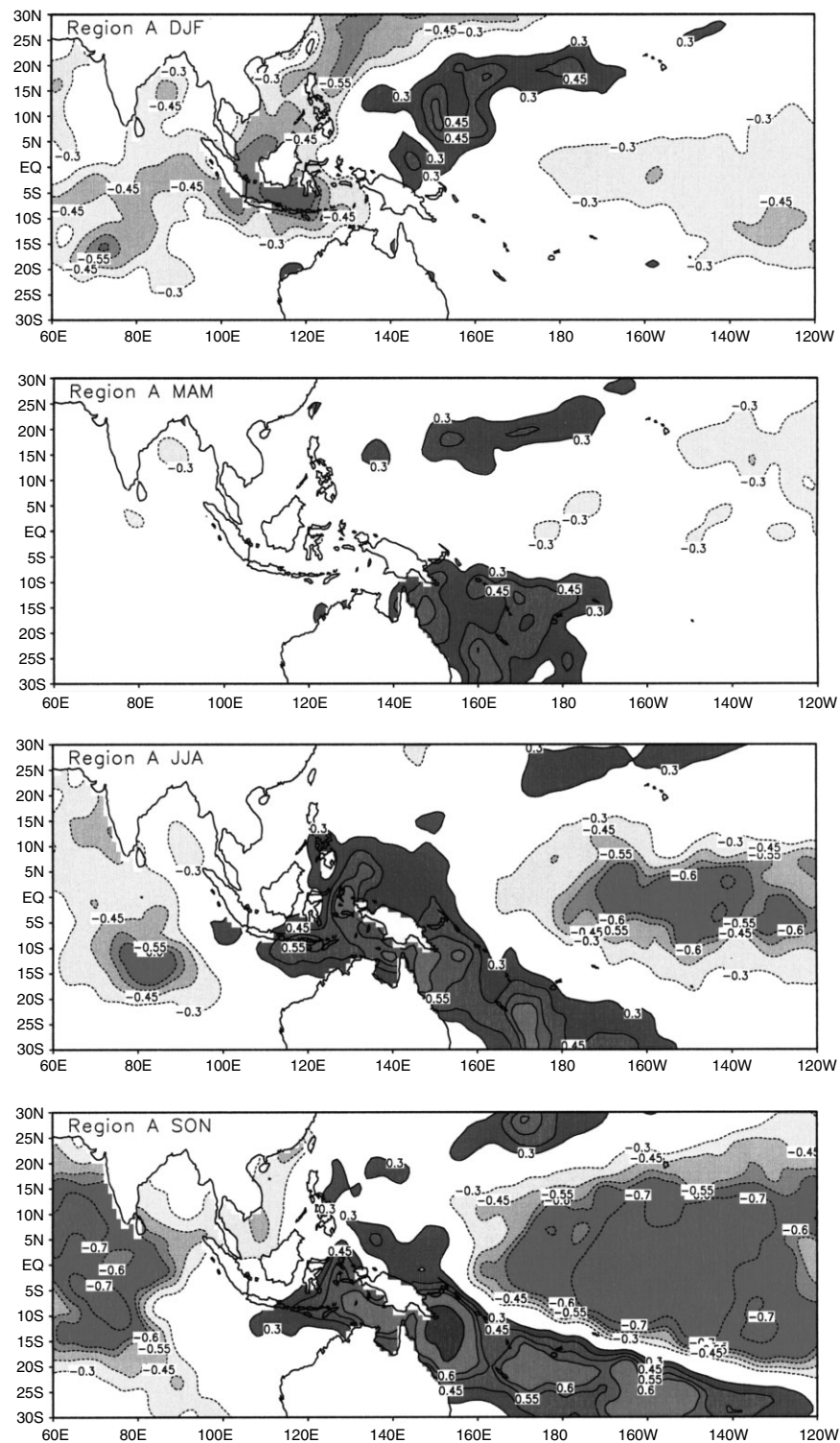
Figure 9. The seasonal correlation of rainfall in Region A against SST. This figure shows correlation values |0.30|, |0.45|, |0.55|, |0.6| and |0.70|, the first three of which correspond to the 90%, 99% and 99.9% significance levels for 33 years of the seasonal correlation

For Region A, the rainfall responses to SST are given in Figure 9. In DJF there are significant negative correlations of rainfall to local SST (< -0.3) in the adjacent Indian Ocean and over Indonesia, from the South China Sea to the Banda Sea. The pattern indicates a relation to the Asian winter monsoon and the location of the ITCZ. Positive correlations exist for some parts in the central Pacific. In MAM, significant positive correlations exist east of Australia and in some parts of the northwestern Pacific. In JJA, the map shows two dipoles of correlation values. One is designated by opposite correlations between the maritime continent (positive) and the equatorial Indian Ocean (negative), and the other dipole is between the maritime continent again and the equatorial western Pacific. Positive correlations exist for the warm pool area, eastern Indonesia seas and the South Pacific convergence zone (SPCZ). Negative correlations exist for the NIÑO3 region and some parts of the Indian Ocean. In SON these dipoles become stronger, with correlation values above |0.7|. In general, except in MAM, Region A experiences positive local SST influences on rainfall but also strong negative influences of ENSO and positive influences of SPCZ in JJA and SON. The responses to both phenomena are stronger in SON.

Region B, as shown in Figure 10, exhibits only a weak rainfall response to SST all year. There are only a few strongly positive responses in SON to SST in the western Pacific. Again, the weakest spatial pattern emerges for MAM. The result is consistent with the analysis of local SST (Figure 8). Region B does not respond to ENSO at all, as already shown by a small amplitude in the rainfall spectrum for the ENSO time scale (Figure 6).

Figure 11 shows the seasonal rainfall response in Region C to SST. In DJF, significant signals exist in the western equatorial Pacific and the Indian Ocean. The response distribution in DJF is much wider and stronger than for Region A. The response in MAM is again the weakest, but stronger than for the other two regions. Strong signals appear in JJA and SON. In JJA, the spatial pattern shows smaller positive areas compared with Region A. However, the strongly negative western Pacific ENSO responses in JJA are stronger than in Region A. Thus, Region C is more strongly influenced by ENSO in JJA than Region A. However, the response to the Indian Ocean SST in JJA is smaller in Region C than in A. In spite of their opposite annual rainfall cycles, the SON responses in Regions C and A are alike, with two strong dipoles at the equator.

In general, MAM is the most unresponsive season, with the least significant correlation values in all three regions. The rainfall of Regions A and C responds significantly negatively (< -0.55) to ENSO events from June to November (an additional response exists in DJF for Region C). The confirmation of the seasonal or monthly variations of rainfall in all regions during ENSO events needs further investigations. The high correlation from June to November in most parts of Indonesia suggests a good possibility for seasonal prediction using SST values. It may be possible to extend the prediction on a monthly basis, especially from June to November. Haylock and McBride (2001) showed that, with regard to the relation of the all-Indonesian rainfall index (63 stations) to the southern oscillation index (SOI) during 1950–98, the wet season (DJF) rainfall in Indonesia is inherently unpredictable. Nicholls (1981) presented evidence that interannual fluctuations of early wet-season rainfall in the Indonesian archipelago can be successfully predicted from prior observations of atmospheric pressure anomalies. It is shown that this predictability is related to SST anomalies.

Two strong dipoles in SON, or boreal fall, are associated to the atmospheric teleconnection between the Pacific and the Indian Oceans, or the Walker cell, which is a tropical atmospheric phenomenon centred in the warm pool near Indonesia. The redistribution of atmospheric mass between the dipoles of the Walker cell plays an important role in determining rainfall variability in the western Pacific and the maritime continent (McGregor, 1992). Arpe *et al.* (1998) suggested that SSTs over the northern Indian Ocean are partly forced by SSTs over the tropical Pacific through ENSO-related atmospheric forcing. The teleconnection strengthens during an El Niño event and the teleconnection causes a dipole-like variability in the Indian Ocean. In a non-ENSO year, a dipole-like SST anomaly pattern exists in the boreal fall season, which can be explained by atmospheric forcing (Baquero-Bernal *et al.*, 2002). Hendon (2003) found that Indonesian rainfall is highly coherent with local and remote SSTs from May to October, and especially in September. Hendon (2003) also mentioned an active Walker cell teleconnection between the Pacific Ocean and the Indian Ocean via Indonesia between September and November as shown in our two dipoles.
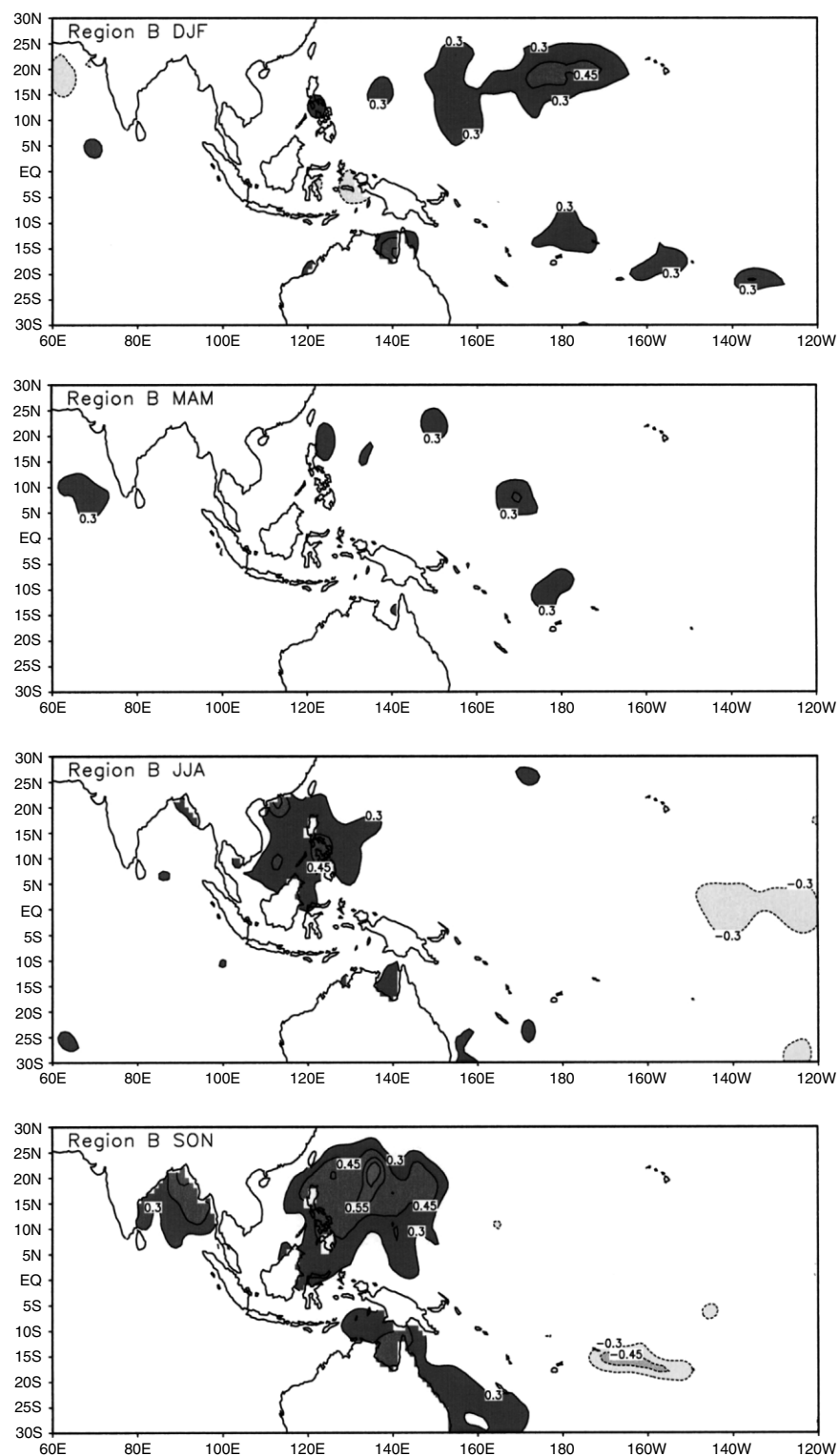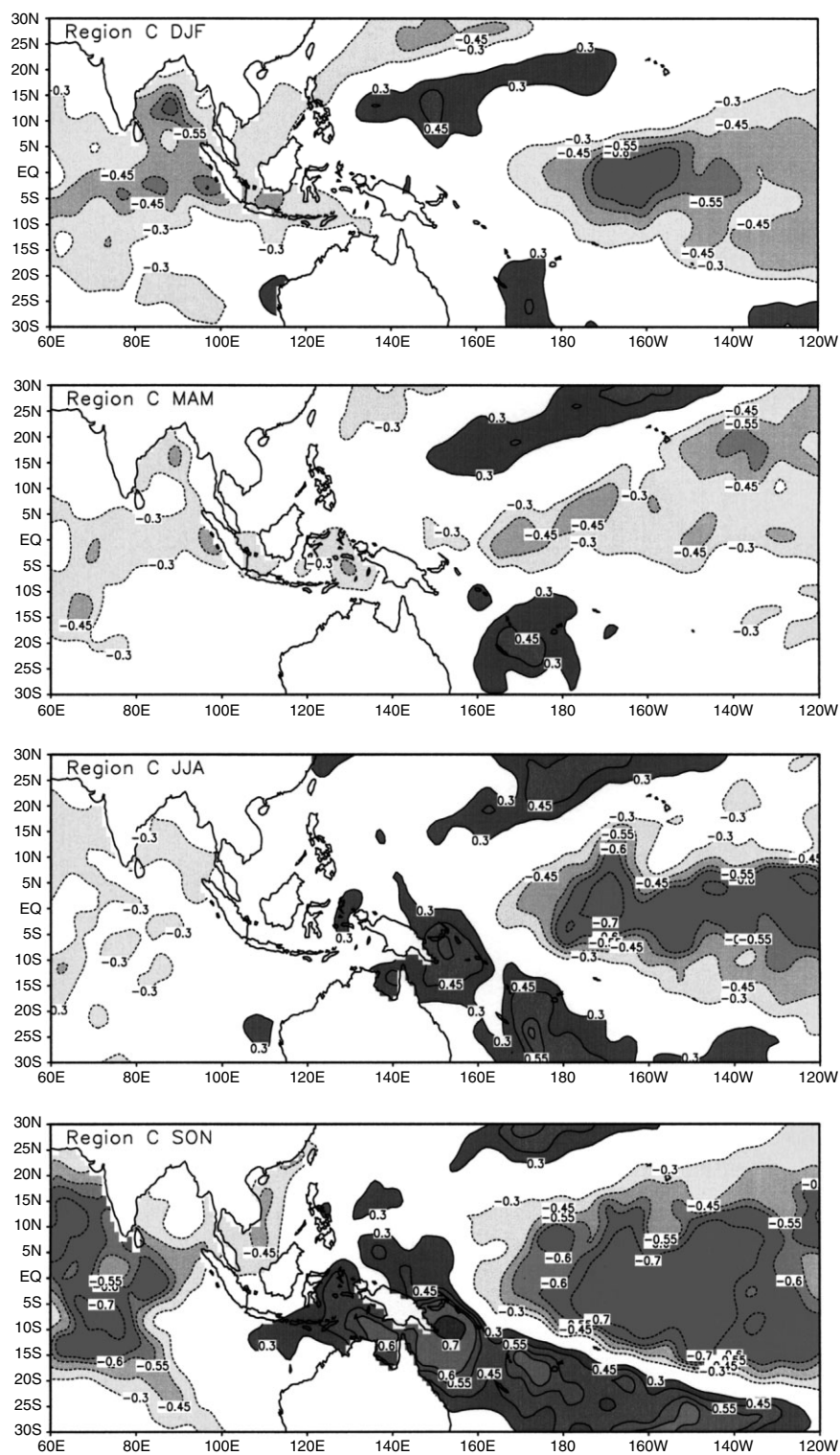
Figure 10. As Figure 9, but for Region B

Figure 11. As Figure 9, but for Region C

4. DISCUSSION AND CONCLUDING REMARKS

We applied a regionalization method, the DCM, to investigate the rainfall variability in the Indonesian archipelago. With DCM, Indonesian rainfall climate can be divided into three clearly distinct regions. Comparisons between the DCM and the EOF and rotated EOF (VARIMAX) methods were undertaken by analysing their spatial patterns and spectra. Since the DCM gives strong annual and semi-annual signals, the analysis of rainfall responses to the ocean was also addressed. The analysis focused on monthly and seasonal responses to the local and remote seas.

The DCM is reliable in isolating regions with a specific annual cycle of precipitation. The method is simple and flexible. One can adjust the threshold correlation value to one's needs and use for other criteria. The resulting regions can have any shape. The spatial pattern of PC1 derived from the EOF and VARIMAX methods resembles, to some degree, regions found by the DCM. Some limitations of the EOF method include patterns that are not dominant (they only explain 30.1% of all variance) and that have no clear boundaries. The DCM also provides a better spectrum in comparison with the other methods, both for the spectrum of each region and for all-Indonesian rainfall. The spectra from the DCM show strong annual and semi-annual signals, as is the case of the spectrum for all-Indonesian rainfall. The VARIMAX method produces similar spectra to the all-Indonesian one and a similar boundary (PC2) for Region B to the DCM.

The DCM delineates three distinct regions of Indonesia with a characteristic annual cycle of precipitation. Region A, the southern and central part of Indonesia influenced by the SE (Australian) monsoon; Region B, the northwestern part of Indonesia with two precipitation peaks per year; and Region C, the Maluku region (the eastern route of the ITF). Except for Region C, all other parts of Indonesia experience strong influences from the Asian monsoon or ITCZ.

Region B has remarkably small standard deviations and strong annual and semi-annual signals in its spectrum and does not respond to remote SST. From the diagram of monthly rainfall versus local SST and from the seasonal analysis, there is no consistent feature apparent in this region. The other two regions, however, respond strongly, and thus promise capability for monthly to seasonal climate prediction. This capability is least in MAM or boreal spring. This idea follows the lowest SST responses of each region in MAM compared with other seasons. This phenomenon is known as the spring predictability barrier. The spring predictability barrier refers to a lower skill generally observed for predictions that extend through boreal spring (e.g. see Webster and Yang, 1992; Balmaseda *et al*., 1995; Flügel and Chang, 1998; Latif *et al*., 1998; Goddard *et al*., 2000). Latif and Graham (1992), in a general circulation model experiment, found that, between April and June, the correlation coefficients between observed and predicted SSTs in the Pacific Ocean are much reduced in comparison with other periods, irrespective of when the prediction has been started. Haylock and McBride (2001) found that the correlation between all-Indonesian rainfall index (63 stations) and the SOI is lowest in DJF and MAM and higher for the other two seasons.

The local SST ranges for which rainfall occurs are from 25.7 to 30.5 °C. Region C has the narrowest range of SST and of rainfall variabilities. A narrow range of SST variability is susceptible to the effect of global climate change, which is presently estimated as an increase in the global surface temperature of between 1.4 and 5.8 °C in the next 100 years (Cubasch *et al*. 2001: figure 9.14). The rainfall in this archipelago occurs near the critical temperature of 29.6 °C, above which an increase in SST means a decrease of the rainfall amount. Thus, seasonal and annual cycle changes of rainfall are highly possible in the future for Regions A and C.

Strong negative rainfall responses in Regions A and C to higher SST in the NIÑO3 area (the warm phase of an El Niño event) for Northern Hemisphere summer and autumn (JJASON) lower an already low rainfall, and thus cause drought. On the other hand, during La Niña, or the cold phase, the dry season gets considerably more rainfall. The ENSO influence on Indonesian rainfall lasts only until November, although some other parts of the world may still receive the impact later. Surprisingly, Region B does not experience any ENSO impact. If we look at Figure 2, Regions A and C coincide with the ENSO-affected parts indicated by Ropelewski and Halpert (1987). This paper advances further with the analysis of the seasonal effects of ENSO.

Indonesian rainfall responds strongly to the remote ocean SST in the warm pool, the NIÑO3 and the SPCZ area in Regions A and C. The two dipoles in the rainfall SST response pattern indicate a Walker cell. The two

dipoles show that, with the Walker cell, the variability of precipitation from the Pacific and Indian Oceans is important. Strong activities of this cell, which affect the rainfall pattern in Indonesia, occur especially during the Northern Hemisphere summer (JJA) and autumn (SON). Moreover, this period is the period of intense influence of ENSO. Thus, there is a need for further research regarding the interactions among ENSO, the ITF and the Walker cell and their influences on Indonesian rainfall, which is beyond the scope of this paper.

ACKNOWLEDGEMENTS

REFERENCES

Arpe K, Dümenil L, Giorgetta MA. 1998. Variability of the Indian monsoon in the ECHAM3 model: sensitivity to sea surface temperature, soil moisture, and the stratospheric quasi-biennial oscillation. *Journal of Climate* **11**: 1837–1858.
Balmaseda MA, Davey MK, Anderson DLT. 1995. Decadal and seasonal dependence of ENSO prediction skill. *Journal of Climate* **8**: 2705–2715.
Baquero-Bernal A, Latif M, Legutke S. 2002. On dipolelike variability of sea surface temperature in the tropical Indian Ocean. *Journal of Climate* **15**: 1358–1368.
Bony S, Lau KM, Sud YC. 1997a. Sea surface temperature and large-scale circulation influences on tropical greenhouse effect and cloud radiative forcing. *Journal of Climate* **10**: 2055–2077.
Bony S, Sud Y, Lau KM, Susskind J, Saha S. 1997b. Comparison and satellite assessment of NASA/DAO and NCEP-NCAR reanalysis over tropical ocean: atmospheric hydrology and radiation. *Journal of Climate* **10**: 1441–1462.
Braak C. 1921. Het Climaat van Nederlandsch Indie. Verhandelingen, 8. Magnetic Meteorology Observation, Batavia.
Cubasch U, Meehl GA, Boer GJ, Stouffer RJ, Dix M, Noda A, Senior CA, Raper S, Yap KS. 2001. Projections of future climate change. In *Climate Change 2001: The Scientific Basis. Report of the Intergovernmental Panel on Climate Change*, Houghton JT, Ding Y, Griggs DJ, Noguer M, van der Linden PJ, Dai X, Maskell K, Johnson CA (eds). Cambridge University Press: Cambridge, UK/New York.
Cressman GP. 1959. An operational objective analysis scheme. *Monthly Weather Review* **117**: 765–783.
Davidson NE. 1984. Short-term fluctuations in the Australian monsoon during winter Monex. *Monthly Weather Review* **112**: 1697–1708.
Davidson NE, McBride JL, McAvaney BJ. 1984. Divergent circulations during the onset of the 1978–79 Australian monsoon. *Monthly Weather Review* **112**: 1684–1696.
Dommenget D, Latif M. 2002. A cautionary note on the interpretation of EOFs. *Journal of Climate* **15**: 216–225.
Flügel M, Chang P. 1998. Does the predictability of ENSO depend on the seasonal cycle? *Journal of the Atmospheric Sciences* **55**: 3230–3243.
Goddard L, Mason SJ, Zebiak SE, Ropelowski CF, Basher R, Cane MA. 2000. Current approaches to seasonal to interannual climate predictions. International Research Institute (IRI) technical report 0–1.
Godfrey JS. 1996. The effect of the Indonesian throughflow on circulation and heat exchange with the atmosphere: a review. *Journal of Geophysical Research* **101**: 12 217–12 337.
Gordon A, Fine R. 1996. Pathways of water between the Pacific and Indian Oceans in the Indonesian seas. *Nature* **379**: 146–149.
Gordon AL, Susanto RD, Ffield A. 1999. Throughflow within Makassar Strait. *Geophysical Research Letters* **26**: 3325–3328.
Gutman G, Csiszar I, Romanov P. 2000. Using NOAA/AVHRR products to monitor El Niño impacts: focus on Indonesia in 1997–98. *Bulletin of the American Meteorological Society* **81**: 1189–1205.
Hackert EC, Hastenrath S. 1986. Mechanism of Jawa rainfall anomalies. *Monthly Weather Review* **114**: 745–757.
Hamada JI, Yamanaka MD, Matsumoto J, Fukao S, Winarso PA, Sribimawati T. 2002. Spatial and temporal variations of the rainy season over Indonesia and their link to ENSO. *Journal of the Meteorological Society of Japan* **80**: 285–310.
Haylock M, McBride JL. 2001. Spatial coherence and predictability of Indonesian wet season rainfall. *Journal of Climate* **14**: 3882–3887.
Hendon HH. 2003. Indonesian rainfall variability: impacts of ENSO and local air–sea interaction. *Journal of Climate* **16**: 1775–1790.
Kaiser HF. 1958. The Varimax criterion for analytic rotations in factor analysis. *Psychometrika* **23**: 187–200.
Kirono DGC, Tapper NJ, McBride JL. 1999. Documenting Indonesian rainfall in the 1997/1998 El Niño event. *Physical Geography* **20**: 422–435.
Latif M, Graham NE. 1992. How much predictive skill is contained in the thermal structure of an OGCM? *Journal of Physical Oceanography* **22**: 951–962.
Latif M, Anderson DLT, Barnett TP, Cane MA, Kleeman R, Leetma A, O'Brien J, Rosati A, Schneider E. 1998. A review of the predictability and prediction of ENSO. *Journal of Geophysical Research* **103**: 14 375–14 393.
Lau KM, Wu HT. 1999. Assessment of the impacts of the 1997–98 El Niño on the Asian–Australian monsoon. *Journal of Geophysical Research* **26**: 1747–1750.
Lau KM, Wu HT. 2001. Principal modes of rainfall–SST variability of the Asian summer monsoon: a reassessment of the monsoon–ENSO relationship. *Journal of Climate* **14**: 2880–2895.
Lau KM, Wu HT, Bony S. 1997. The role of large-scale atmospheric circulation in the relationship between tropical convection and sea surface temperature. *Journal of Climate* **10**: 381–392.

McBride JL. 1999. Indonesia, Papua New Guinea, and tropical Australia: the southern hemisphere monsoon. In *Meteorology of Southern Hemisphere*, Karoly DJ, Vincent DG (eds). Meteorological monograph 49. AMS: Boston; 89–98.

McGregor GR. 1992. Temporal and spatial characteristics of coastal rainfall anomalies in Papua New Guinea and their relationship to the southern oscillation. *International Journal of Climatology* **12**: 449–468.

Morey SL, Shriver JF, O'Brien JJ. 1999. The effects of Halmahera on the Indonesian throughflow. *Journal of Geophysical Research* **104**: 23 281–23 296.

Newell RE, Selkirk R, Ebisuzaki W. 1982. The southern oscillation–sea surface temperature and wind relationships in a 100-year data set. *Journal of Climatology* **2**: 357–373.

Nicholls N. 1981. Air–sea interaction and the possibility of long-range weather prediction in the Indonesian archipelago. *Monthly Weather Review* **109**: 2345–2443.

Nicholls N. 1983. Predicting Indian monsoon rainfall from sea-surface temperature in the Indonesian–north Australia area. *Nature* **306**: 576–577.

Nicholls N. 1984. The southern oscillation and Indonesia sea surface temperature. *Monthly. Weather Review* **112**: 424–432.

Nicholls N. 1995. All-India summer monsoon rainfall and sea surface temperature around northern Australia and Indonesia. *Journal of Climate* **8**: 1463–1467.

Peterson TC, Vose R, Schmoyer R, Razuvaev V. 1998. Global Historical Climatology Network (GHCN) quality control of monthly temperature data. *International Journal Climatology* **18**: 1169–1179.

Philander SGH. 1983. El Niño southern oscillation phenomena. *Nature* **302**: 295–301.

Rasmusson EM, Carpenter TH. 1982. Variations in tropical sea surface temperature and surface wind fields associated with the southern oscillation/El Niño. *Monthly Weather Review* **110**: 354–384.

Rayner NA, Horton EB, Parker DE, Folland CK, Hackett RB. 1996. Version 2.2 of the global sea-ice and sea surface temperature data set, 1903–1994. Climate Research Technical Note CRTN74.

Ropelewski CF, Halpert MS. 1987. Global and regional scale rainfall patterns associated with the El Niño southern oscillation (ENSO). *Monthly Weather Review* **115**: 1606–1626.

Shukla J, Paolino DA. 1983. The southern oscillation and long-range forecasting of the summer monsoon rainfall over India. *Monthly Weather Review* **111**: 1830–1837.

Sukanto M. 1969. Climate of Indonesia. In *Climates of Northern and Eastern Asia*, Arakawa H (ed.). World Survey of Climatology, Vol. 8, Elsevier: 215–229.

von Storch H, Zwiers FW. 1999. *Statistical Analysis in Climate Research*. Cambridge University Press: Cambridge.

Vose RS, Schmoyer RL, Steurer PM, Peterson TC, Heim R, Karl TR, Eischeid JK. 1992. The Global Historical Climatology Network: long-term monthly temperature, precipitation, sea level pressure, and station pressure data. ORNL/CDIAC-53, NDP-041.

Webster PJ, Yang S. 1992. Monsoon and ENSO: selectively interactive systems. *Quarterly Journal of the Royal Meteorological Society* **118**: 877–925.

Wyrtki K. 1956. The rainfall over the Indonesian waters. Verhandelingen, 49. Kementrian Perhubungan Lembaga Meteorologi dan Geofisika, Jakarta.

Wyrtki K. 1961. Physical oceanography of the Southeast Asian waters. In *Scientific Results of Maritime Investigations of the South China Sea and Gulf of Thailand 1959–1961. Naga Report 2*. University of California/Scripps Institute of Oceanography: 195pp.